Progress In Electromagnetics Research C, Vol. 48, 167–175, 2014

Design and Study of Uniplanar Coupled Inverted-L Antenna for Single-/Dual-Band Operation

Chao-Shun Yang* **and Christina F. Jou**

Abstract—A coupled-line-based planar antenna for single-band and dual-band operation is presented. The well-known uniplanar coupled inverted-L antenna (UCILA) has a simple and specific mechanism to achieve the dual-band ratio that was not described in the past. The UCILA which shunted a short stub in the slotline portion can provide switchable modes among single-low band (3.4% for WLAN 2.44 GHz), single-high band (15% for WLAN 5.2–5.8 GHz band) and dual-band (WLAN 2.44/5–6 GHz) operations.

1. INTRODUCTION

Regarding the IEEE 802.11a/b/g dual-band antenna design, numerous literatures have been proposed using printed monopole and PIFA designs. The dual-band printed monopole antenna designs used G-shaped, F-shaped, stacked U or stacked T-shaped [1–4] radiators. In these designs, the parasitic elements such as backed rectangular patch, grounded L-strip, radiator coupling with separated L-strip, and sleeve [5–8] were employed. The design used asymmetrical single patch [9]. Structures using asymmetrical single patch [9] and L-strip feeding coupling to the radiator [10, 11] have also be studied. In order to reduce antenna profile, the PIFA topologies for dual-band design used two strips separated with an L-shaped slot [12], double short stub [13], short meandering stub [14], and slit etched onto ground plane [15]. Two miniaturized design, one for spiral-shaped radiator of inductive coupling and the other for radiator of capacitive coupling [16] were proposed. Furthermore, extending PIFA design has been explored to achieve different specifications, such as a shunted F-L radiator with wide-high band [17], a stacked inverted-F radiator with wide-low band [18], and a stacked inverted-FL radiator with grounded inverted-L strip that can reduce the antenna size effectively [19]. A trade-off design was considered for small size and radiation efficiency [20]. In addition, the slotline design has been used for frequency reconfiguration by adding active components in the slotline. A pin-diode in the slotline is regarded as a switch, and the on/off state can control frequency movement [21]. Numerous pin diodes for frequency adjusting were also reported [22]. The RF MEMS switches configuration in loop slot can obtain more freedom in frequency adjustment [23]. The frequency reconfiguration is achieved by using varactors [24], or the combination of pin diodes [25].

In Section 2, the proposed antenna design combined with dual-band and frequency-switching property consists of the prototype UCILA and a shunted open-circuited slotline (OCS) with movable ground plane which can achieve dual-band bandwidth, single-low band or single-high band. In order to facilitate fabrication and measurement, the OCS end filled with shorting ground plane forms a shunted short-circuited slotline (SCS), and a short stub in the SCS can achieve the frequency switching property. In addition, the well-known prototype UCILA (similar to [26]) consisting of double inverted-L line can provide a simple dual-band mechanism to achieve the required dual-band ratio. The dual-band mechanism controlled by the UCILA length for central-stop frequency shifting and the UCILA gap

Received 23 February 2014, Accepted 25 March 2014, Scheduled 26 March 2014

* Corresponding author: Chao-Shun Yang (9613806.cm96g@g2.nctu.edu.tw).
The authors are with the Institute of Communications Engineering, National Chiao-Tung University, Taiwan.

for dual-band ratio is not discussed in the past literature. The antenna pattern, gain and radiation efficiency of the first antenna design is introduced. Furthermore, the proposed lumped-circuit model is used to investigate the average input-power ratio between UCILA and SCS near the discussed resonant frequency at 5.2 GHz. By means of the measured radiation efficiency and lumped-circuit model, the radiating power between UCILA and SCS can be obtained. Section 3 is the conclusion.

2. THE ANTENNA DESIGN

2.1. The Prototype of the Single-/Dual-Band Switching Antenna

Figure 1(a) shows the structural parameters of the antenna design including UCILA length ℓ_s = 10.7 mm, UCILA *gap* = 1 mm and the 25 mm length of the shunted open-circuited slotline (OCS). Figure 1(b) shows the structural dimensions in detail. The dual-band mechanism will be described in Section 2.3. Note that the ground plane edge and movable metallic plate edge can be considered as a short circuited resonant cavity. The distance between these two edges is defined as ℓ. The antenna can be switched between single-low frequency operation and single-high frequency operation by adjusting the length ℓ. Figure 2 shows the WLAN low-band operation for ℓ = 3 mm, the WLAN high-band operation for ℓ = 17 mm and WLAN dual-band operation for ℓ = 25 mm (open slotline).

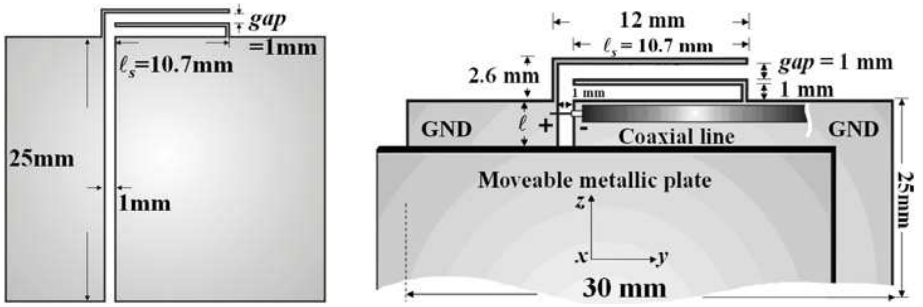

Figure 1. The antenna design for frequency-switching design. (a) The UCILA with the OCS. (b) The UCILA with the MMP.

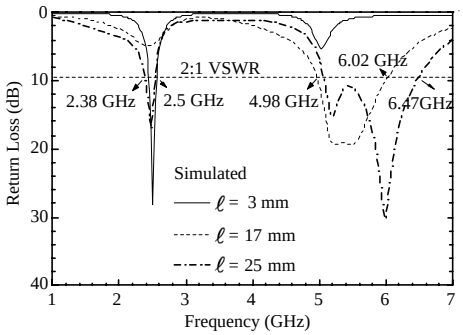

Figure 2. The simulated return loss of the antenna design.

2.2. The Realization of the Single-/Dual-Band Switching Antenna

A simple equivalent method can replace the MMP movement (a mechanical device) to facilitate the fabrication. The end of the OCS is filled with the shorting plane, which forms a short-circuited slotline (SCS) with a short stub in it. The antenna structure is shown in Figure 3. The UCILA area is 12 mm × 2.6 mm, and the ground plane area is 30 mm × 25 mm, while both centers of the UCILA and

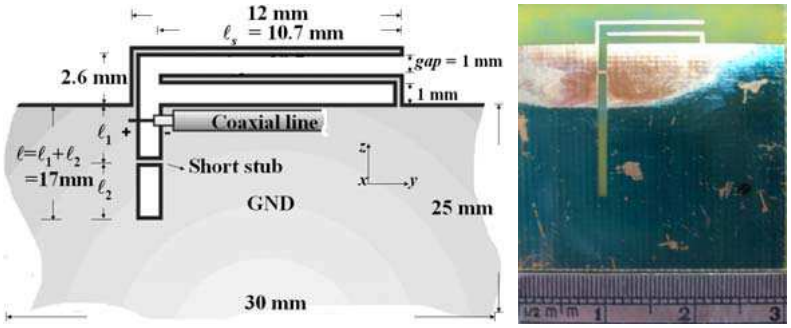

Figure 3. The proposed antenna design. (a) The antenna dimension and structural parameter. (b) The photograph.

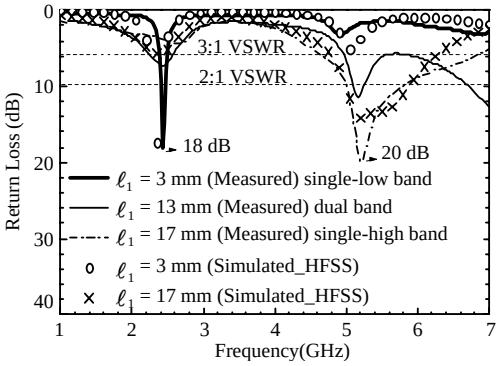

Figure 4. The return loss of the proposed antenna design for the parameter-ℓ_1 variation.

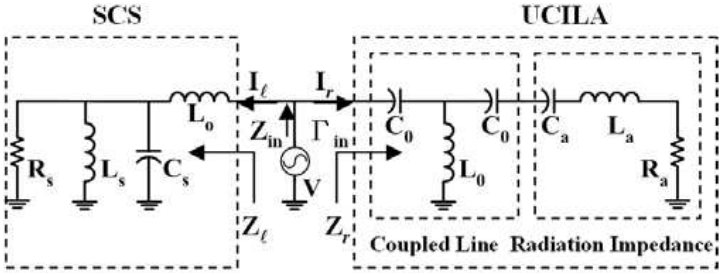

Figure 5. The lumped-circuit model of the UCILA with the shunted SCS.

ground plane are aligned. All the antennas presented in this paper are fabricated on a FR4 epoxy substrate with thickness of 0.8 mm, relative dielectric constant of 4.4, and loss tangent of 0.02. The characteristic impedance of slotline is 106 Ω, and the effective dielectric constant is 1.7. A short stub ℓ_1 is located in the SCS length $\ell = 17$ mm ($= 0.17\lambda_g$ at 2.44 GHz, $= 0.41\lambda_g$ at 5.5 GHz), where $\ell = \ell_1 + \ell_2$. According to the simulated and measured return losses shown in Figure 4, the short stub $\ell_1 = 3$ mm can achieve a single low-band operation in 2400–2484 MHz under VSWR $\leqq 2$. Meanwhile, the short stub $\ell_1 = 13$ mm can achieve a dual-band operation in 2400–2483.5 MHz and 5–6 GHz under VSWR $\leqq 3$. The short-stub $\ell_1 = 17$ mm can achieve a single high-band operation in 5000–5854 MHz under VSWR $\leqq 2$.

Figure 5 shows the lumped-circuit model of the antenna near the resonant frequency. The radiation impedance (series-RLC resonant circuit) and dual-band property (T-model circuit) of the UCILA can be illustrated in the UCILA dash-line frame shown in Figure 5. The SCS cavity (parallel RLC resonant circuit with a compensated series inductance) can be illustrated in the SCS dash-line frame shown in

Figure 5. The RLC-value extraction of the short-stub ℓ_1 variation is demonstrated in Section 2.4 to explain the average input-power ratio between UCILA and SCS.

2.3. The Dual-Band Mechanism of the UCILA

Figure 6 shows the uniplanar coupled inverted-L antenna (UCILA). For the UCILA structure, when port 1 is feeding, port 2 and port 4 are open, and port 3 is terminated with 50 Ω. It is a quarter-wave resonator in the resonant frequency f_c according to the microwave filter theory [27]. Therefore, the UCILA length (ℓ_s) can determine the resonant frequency f_c. An experienced formula is in the following (1), where c is for light velocity and $\varepsilon^c_{eff}/\varepsilon^\pi_{eff}$ the effective dielectric constant of the common/differential mode of the coupled line.

$$f_c = c \Big/ \left(4\ell_s \frac{\sqrt{\varepsilon^c_{eff}} + \sqrt{\varepsilon^\pi_{eff}}}{2} \right) \tag{1}$$

When the port 3 is short to ground plane, and the resonant frequency f_c becomes a stop frequency and splits two modes (f_1 and f_2) based on the coupling magnitude. Figure 7 shows that the current

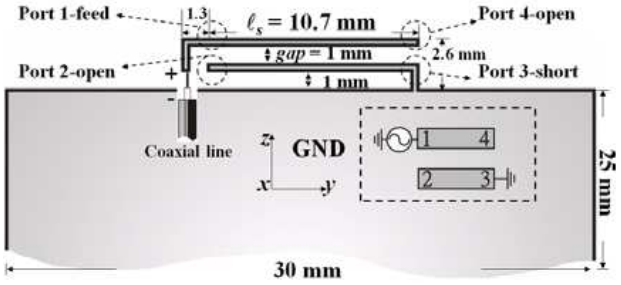

Figure 6. The antenna prototype, uniplanar coupled inverted-L antenna (UCILA).

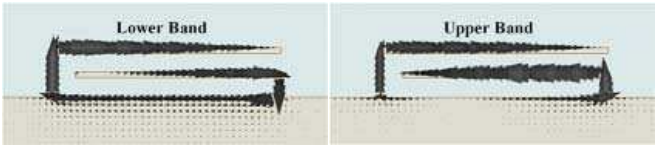

Figure 7. The UCILA current distribution. (a) Lower band in the common mode. (b) Upper band in the differential mode.

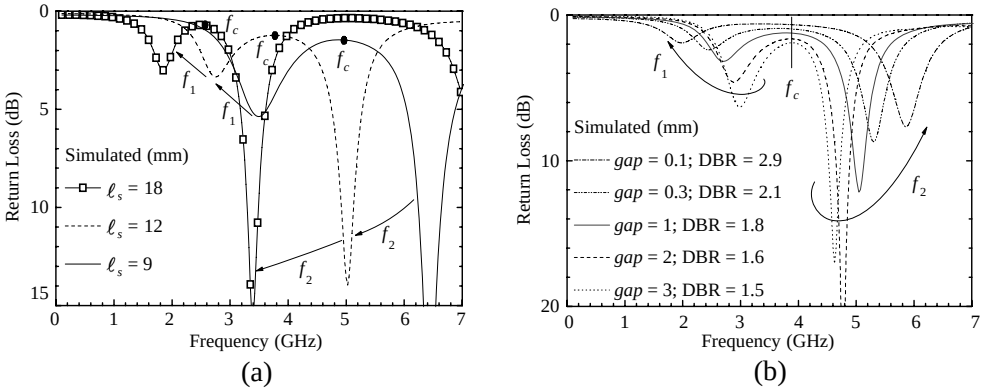

Figure 8. The dual-band mechanism. (a) Central-strop frequency shifting and (b) dual-band ratio.

distribution of the lower band (f_1) is in the common mode, and that of the upper band (f_2) is in the differential mode [28]. The strong coupling is due to the decreasing coupled-line gap which makes the f_1 toward low frequency and the f_2 toward high frequency. Therefore, the parameter ℓ_s and *gap* can determine the central-stop frequency (f_c) and the dual-band ratio (DBR = f_2/f_1).

In Figure 8, the full-wave solver was utilized to simulate how coupled-line length ℓ_s controls the f_c carrying f_1 and f_2, and how coupled-line gap controls the dual-band ratio. In Figure 8(a), the f_c is shifted toward low frequency carrying f_1 and f_2 in the same dual-band ratio about 1.8 by increasing antenna length ℓ_s. In Figure 8(b), the DBR can be adjusted by the coupled-line *gap* from the fixed central-stop frequency f_c. Note that the decreasing gap from 3 mm to 0.1 mm results in the rise of DBR from 1.5 to 2.9.

2.4. The Radiation Characteristic of the Single-/Dual-Band Switching Antenna

Here, the antenna pattern, gain and radiation efficiency of the proposed antenna design are introduced. Furthermore, the proposed lumped-circuit model is used to investigate the average input-power ratio between UCILA and SCS near the discussed resonant frequency at 5.2 GHz. By means of the measured radiation efficiency and lumped-circuit model, the radiating power between UCILA and SCS can be obtained. Note that the lumped circuit model does not predict the same bandwidth as the simulated result. This deviation is attributable to the fact that mutual coupling between UCILA and SCS cannot be considered.

Figures 9(a) and 9(b) show that the electric field of the UCILA with the shunted SCS is E_θ and E_ϕ, which are generated by the y-direction electric current of the UCILA and the z-direction magnetic current of the shunted SCS, respectively. The z-direction magnetic current is equivalent to the surrounded slotline current. Figure 10(a) shows the radiation pattern of the UCILA with the short stub $\ell_1 = 3$ mm at 2.44 GHz, and Figure 10(b) shows the radiation pattern of the UCILA with the short stub $\ell_1 = 17$ mm at 5.5 GHz. Note that the E_ϕ level is obviously larger than E_θ in the x-z plane at the 5.5 GHz due to the SCS without the short stub. Antenna peak gain and radiation efficiency are shown in Figure 11. The UCILA with the short stub $\ell_1 = 3$ mm has a peak gain of 1.1 dBi and radiation efficiency of 55% at 2.44 GHz. The UCILA with the short stub $\ell_1 = 17$ mm has a peak gain of 4.8 dBi and radiation efficiency of 93% at 5.5 GHz.

The lumped-circuit model is employed to explain the average input-power ratio between UCILA and SCS. For the single low-band design of the UCILA with the short stub $\ell_1 = 3$ mm (see Figure 3), there are two reasons to state that the power consumption is mainly from the UCILA (radiating resistance) rather than SCS (shorting). The first reason is that the short stub $\ell_1 = 3$ mm ($0.03\lambda_g$) is much smaller than slotline at 2.44 GHz, which can be considered as an inductor or the shorting stripline of PIFA. The second reason is that the current distribution shown in Figure 9(a), which is mainly confined between

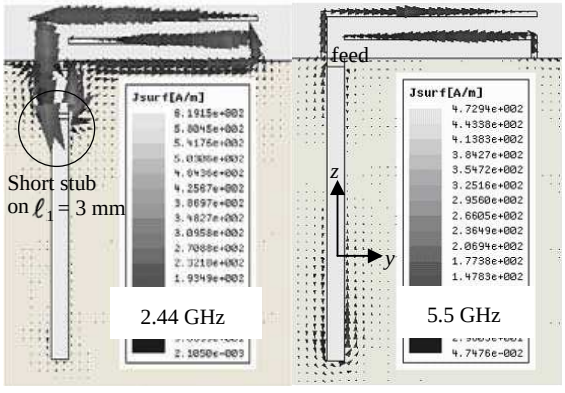

Figure 9. The surface current distribution. (a) The UCILA with the short stub ℓ_1= 3 mm in the common mode at 2.44 GHz. (b) The UCILA with a short stub $\ell_1 = \ell = 17$ mm in the differential mode at 5.5 GHz.

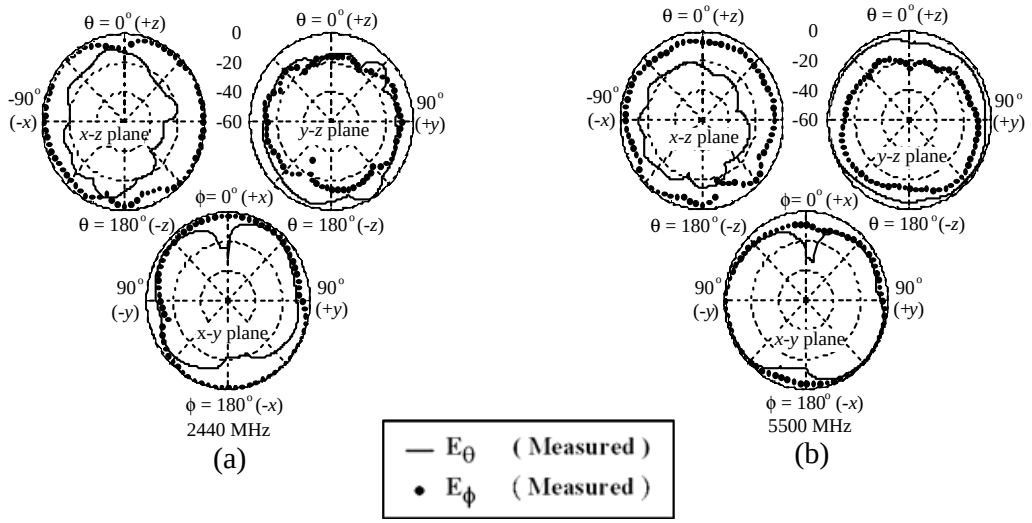

Figure 10. Antenna radiation pattern. (a) The UCILA with the short-stub $\ell_1 = 3\,\text{mm}$ at 2.44 GHz. (b) The UCILA with a short stub $\ell_1 = \ell = 17\,\text{mm}$ at 5.5 GHz.

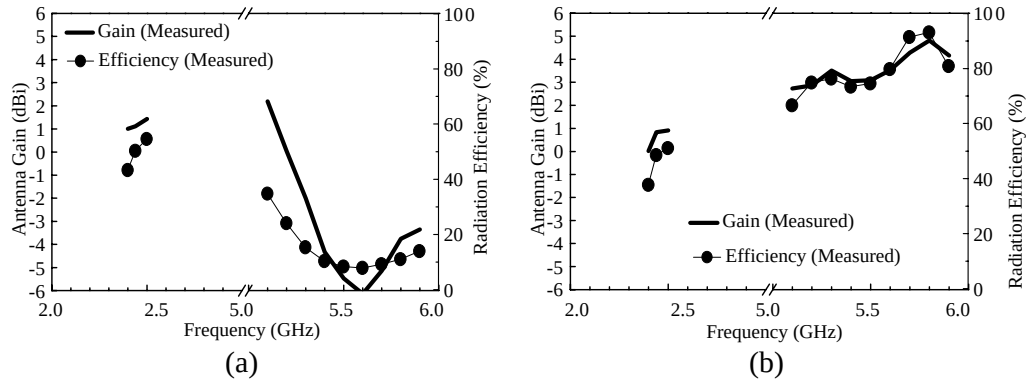

Figure 11. Antenna peak gain and radiation efficiency. (a) The UCILA with the short stub $\ell_1 = 3\,\text{mm}$ in the shunted SCS. (b) The UCILA with a short stub $\ell_1 = \ell = 17\,\text{mm}$ in the shunted SCS.

the UCILA and the short-stub ℓ_1, has a few surrounded current in slotline ℓ_2. Therefore, the slotline ℓ_2 is similar to a full-filled ground plane. However, for the single high-band design of the UCILA with short stub $\ell_1 = \ell = 17\,\text{mm}$ (see Figure 3), it can be divided into UCILA and SCS. Figure 5 shows that the UCILA can be considered as a two-port component connected between feeding and series-RLC radiation impedance. The radiation impedance $R_a = 75\,\Omega/L_a = 30\,\text{nH}/C_a = 55\,\text{fF}$ is extracted by the full-wave solver via embedding the feeding transverse plane along the uniform coupled line to the open-end plane. The two-port component can be modeled as a transmission-line $Z_0 = 270\,\Omega$ and the electric length is 128° at 5.2 GHz, which can be extracted as the T-model $C_0 = 0.2324\,\text{pF}/L_0 = 10.4869\,\text{nH}$ [27]. Figure 12(a) shows that the input impedance of the UCILA is composed of the T model and the radiation impedance. In Figure 12(b), the SCS ($\ell_1 = 17\,\text{mm}$) is a short-circuited cavity that is composed of a parallel $R_s = 3594\,\Omega/L_s = 6.8\,\text{nH}/C_s = 0.4194\,\text{pF}$ and a compensated $L_o = 2\,\text{nH}$. Figure 12(c) shows the measured and simulated return loss of the complete circuit consisting of the UCILA and SCS. Therefore, the lumped-circuit model can estimate the average input power from UCILA and SCS near the resonant frequency 5.2 GHz. Note that the mutual coupling between UCILA and SCS cannot be modeled, so the bandwidth cannot be accurately estimated.

After demonstrating the input impedance and return loss of the lumped-circuit model, the average input-power ratio is formulated in the following. The input impedance is Z_ℓ for SCS and is Z_r for

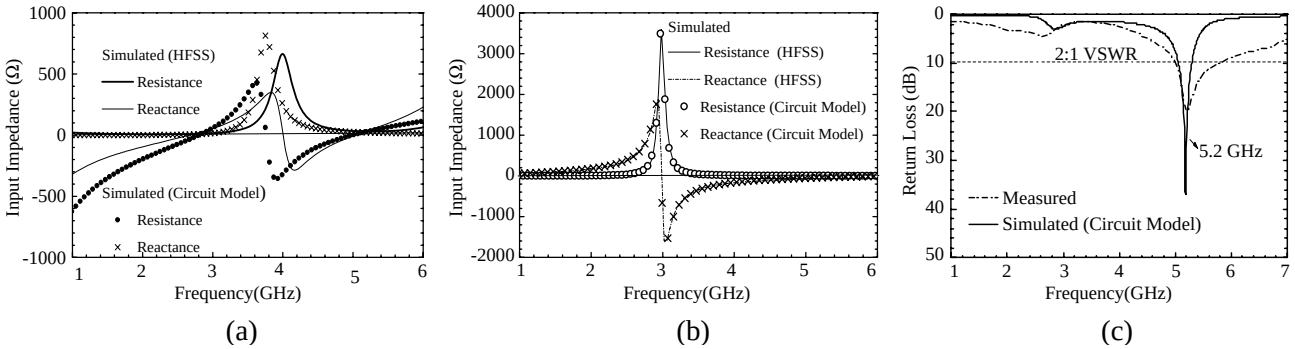

Figure 12. (a) The input impedance of the UCILA. (b) The input impedance of SCS. (c) The return loss of the UCILA with the shunted SCS.

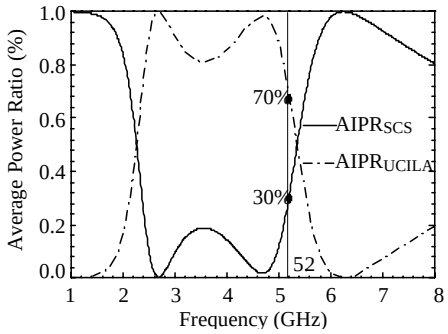

Figure 13. The average input-power ratio of the UCILA and SCS.

UCILA in (2)–(3), respectively. Hence, the total input impedance Z_{in} and reflction coefficient Γ_{in} can be obtained from Z_ℓ and Z_r shown in (4)–(5). The $Z_s = 50\,\Omega$ is system impedance. The input voltage V and current I are listed in (6)–(7) by given a voltage source $v_{\text{in}} = 1$ volt.

$$Z_\ell = 1/\left(1/R_m + j\omega C_m + 1/(j\omega L_m)\right) + j\omega L_c \tag{2}$$

$$Z_r = 1 \Big/ \left(\frac{1}{R_a + j\omega L_a + 1/(j\omega C_a) + 1/(j\omega C_0)} + \frac{1}{j\omega L_0}\right) + \frac{1}{j\omega C_0} \tag{3}$$

$$Z_{\text{in}} = \frac{Z_\ell Z_r}{Z_\ell + Z_r} \tag{4}$$

$$\Gamma_{\text{in}} = \frac{Z_{\text{in}} - Z_s}{Z_{\text{in}} + Z_s} \tag{5}$$

$$V = v_{\text{in}}(1 + \Gamma_{\text{in}}), \quad v_{\text{in}} = 1 \tag{6}$$

$$I = V/Z_{\text{in}} \tag{7}$$

The current toward the UCILA is I_r, and the current toward the SCS is I_ℓ in (8). According to the average power definition, the average powers of the UCILA and SCS are P_r and P_ℓ in (9), respectively. In Figure 13, the average input-power ratio $\text{AIPR}_{\text{UCILA}}$ and AIPR_{SCS} in (10) can be used to identify the input-power consumption. The input-power consumptions are 70% and 30% from UCILA and SCS near the resonant frequency 5.2 GHz, respectively. Therefore, at the 2.44 GHz, the dominant radiating power is contributed from UCILA about 44% due to the product of radiation efficiency (50%) and return loss (87.5% incident power = 18 dB, see Figure 4). At 5.2 GHz, the radiating powers contributed from UCILA and SCS are about 47% and 20% due to the product of radiation efficiency (75%) and average input-power ratio (70/30%) and return loss (90% incident power = 20 dB, see Figure 4). Note that the SCS occupies larger area, but its radiating power is less than UCILA. Therefore, the UCILA

is the major radiator.

$$I_r = IZ_\ell/(Z_r + Z_\ell), \quad I_\ell = IZ_r/(Z_r + Z_\ell) \tag{8}$$

$$P_r = \tfrac{1}{2}\mathrm{Re}\{V \cdot I_r^*\}, \quad P_\ell = \tfrac{1}{2}\mathrm{Re}\{V \cdot I_\ell^*\} \tag{9}$$

$$\mathrm{APR}_{\mathrm{UCILA}} = P_r/(P_r + P_\ell) \quad , \quad \mathrm{APR}_{\mathrm{scs}} = P_\ell/(P_r + P_\ell) \tag{10}$$

3. CONCLUSION

In this paper, the well-known UCILA is investigated, which has simple and specific dual-band mechanism. The proposed antenna design utilizing UCILA with a short stub in the shunted SCS can select single-low (802.11b/g) or single-high band (802.11a), or dual band (802.11a/b/g). The peak gain and radiation efficiency of single-low band at 2.44 GHz is 1.1 dBi and 55%, and the peak gain and radiation efficiency of single-high band at 5.5 GHz are 4.8 dBi and 93%.

REFERENCES

1. Pan, C. Y., C. H. Huang, and T. S. Horng, "A novel printed G-shaped monopole antenna far dual-band WLAN applications," *IEEE AP-S Int. Symp.*, Vol. 3, 3099–3102, Jun. 20–25, 2004.
2. Yeh, S.-H. and K.-L. Wong, "Dual-band F-shaped monopole antenna for 2.4/5.2 GHz WLAN application," *IEEE AP-S Int. Symp.*, Vol. 4, 72–75, Jun. 16–21, 2002.
3. Chen, I.-F. and C.-M. Peng, "Microstrip-fed dual-U-shaped printed monopole antenna for dual-band wireless communication applications," *Electronics Lett.*, Vol. 39, No. 13, 955–956, Jun. 2003.
4. Kuo, Y.-L. and K.-L. Wong, "Printed double-T monopole antenna for 2.4/5.2 GHz dual-band WLAN operations," *IEEE Trans. Antennas Propagat.*, Vol. 51, 2187–2192, Sep. 2003.
5. Pan, C.Y., C. H. Huang, and T. S. Horng, "A novel printed monopole antenna with a square conductor-backed parasitic plane for dual-band WLAN applications," *IEEE AP-S Int. Symp.*, Vol. 1, 261–264, Jun. 20–25, 2004.
6. Wong, K.-L., L.-C. Chou, and C.-M. Su, "Dual-band flat-plate antenna with a shorted parasitic element for laptop applications," *IEEE Trans. Antennas Propagat.*, Vol. 53, No. 1, 539–544, Jan. 2005.
7. Jan, J.-Y., L.-C. Tseng, W.-S. Chen, and Y.-T. Cheng, "Printed monopole antennas stacked with a shorted parasitic wire for Bluetooth and WLAN applications," *IEEE AP-S Int. Symp.*, Vol. 3, 2607–2610, Jun. 20–25, 2004.
8. Wu, J.-W., H.-M. Hsiao, J.-H. Lu, and Y.-D. Wang, "Dual-broadband T-shaped monopole antenna for wireless communication," *IEEE AP-S Int. Symp.*, Vol. 1A, 470–473, Jul. 3–8, 2005.
9. Chen, H.-M. and Y.-F. Lin, "Printed monopole antenna for 2.4/5.2 GHz dual-band operation," *IEEE AP-S Int. Symp.*, Vol. 3, 60–63, Jun. 22–27, 2003.
10. Wang, Y.-Y. and S.-J. Chung, "A new dual-band antenna for WLAN applications," *IEEE AP-S Int. Symp.*, Vol. 3, 2611–2614, Jun. 20–25, 2004.
11. Lee, C.-T. and K.-L. Wong, "Uniplanar printed coupled-fed PIFA with a band-notching slit for WLAN/WiMAX operation in the laptop computer," *IEEE Trans. Antennas Propagat.*, Vol. 57, No. 4, 1252–1258, Apr. 2009.
12. Angelopoulos, E. S., A. I. Kostaridis, and D. I. Kaklamani, "A novel dual-band F-inverted antenna printed on a PCMCIA card," *Microwave Opt. Technol. Lett.*, Vol. 42, No. 2, 153–156, Jul. 2004.
13. Liu, H.-W., S.-Y. Lin, and C.-F. Yang, "Compact inverted-F antenna with meander shorting strip for laptop computer WLAN applications," *IEEE Antennas and Wireless Propagat. Lett.*, Vol. 10, 540–543, 2011.
14. Chan, P. W., H. Wong, and E. K. N. Yung, "Dual-band printed inverted-F antenna for DCS, 2.4 GHz WLAN applications," *Proc. LAPC*, 185–188, Loughborough, UK, Mar. 17–18, 2008.
15. Razali, A. R., M. E. Bialkowski, and F.-C. E. Tsai, "Multi-band planar inverted-F Antenna with microstripline coupling to open-end ground slots," *Proc. Asia-Pacific Microwave Conf.*, 2471–2474, Dec. 17–18, 2009.

16. Wang, Y.-S., M.-C. Lee, and S.-J. Chung, "Two PIFA-related miniaturized dual-band antennas," *IEEE Trans. Antennas Propagat.*, Vol. 55, No. 3, 805–811, Mar. 2007.
17. Sim, D.-U. and J.-I. Choi, "A compact wideband modified planar inverted F antenna (PIFA) for 2.4/5-GHz WLAN applications," *Antennas and Wireless Propagat. Lett.*, Vol. 5, 391–394, 2006.
18. Kuo, Y.-L., T.-W. Chiou, and K.-L. Wong, "A novel dual-band printed inverted-F antenna," *Microwave Opt. Technol. Lett.*, Vol. 31, No. 5, 353–355, Dec. 2001.
19. Nakano, H., Y. Sato, H. Mimaki, and J. Yamauchi, "An inverted FL antenna for dual-frequency operation," *IEEE Trans. Antennas Propagat.*, Vol. 53, No. 8, 2417–2421, Aug. 2005.
20. Liu, Y., J. Lee, K. Jung, and H. Kim, "Dual-band PIFA using resonated loop feed structure," *Electronics Lett.*, Vol. 48, No. 6, 309–310, Mar. 2012.
21. Saghati, A. P., M. Azarmanesh, and R. Zaker, "A novel switchable single- and multifrequency triple-slot antenna for 2.4-GHz bluetooth, 3.5-GHz WiMAX, and 5.8-GHz WLAN," *IEEE Antennas and Wireless Propagat. Lett.*, Vol. 9, 534–537, 2010.
22. Razali, A. R. and M. E. Bialkowski, "Investigation into a size-reconfigurable ground slot for multiband folded coplanar inverted-F antenna," *Proc. Asia-Pacific Microwave Conf.*, 1310–1313, Dec. 5–8, 2011.
23. Chiu, C.-Y., J. Li, S. Song, and R. D. Murch, "Frequency-reconfigurable pixel slot antenna," *IEEE Trans. Antennas Propagat.*, Vol. 60, No. 10, 4921–4924, Oct. 2012.
24. Behdad, N. and K. Sarabandi, "A varactor-tuned dual-band slot antenna," *IEEE Trans. Antennas Propagat.*, Vol. 54, No. 2, 401–408, Feb. 2006.
25. Li, H., J. Xiong, Y. Yu, and S. He, "A simple compact reconfigurable slot antenna with a very wide tuning range," *IEEE Trans. Antennas Propagat.*, Vol. 58, No. 11, 3725–3728, Nov. 2010.
26. Wong, K.-L., Y.-W. Chang, and S.-C. Chen, "Bandwidth enhancement of small-size planar tablet computer antenna using a parallel-resonant spiral slit," *IEEE Trans. Antennas Propagat.*, Vol. 60, No. 4, 1705–1711, Apr. 2012.
27. Pozar, D. M., *Microwave Engineering*, 3nd Edition, Chapter 8, Wiley, New York, 2005.
28. Hong, J.-S. and M. J. Lancaster, *Microstrip Filters for RF/Microwave Applications*, Chapter 8, Wiley, New York, 2001.